Celal Bayar University Journal of Science

Coffee Active Ingredient Loaded Biopolymer Nanoparticles: Synthesis and Characterization

Özge Vardar[1], Ayça Mehmetoğlu Al[2], Yeliz Yıldırım [1,3]*

[1] Department of Chemistry, Faculty of Science, Ege University, Izmir, Türkiye
[2] Department of Biotechnology, Graduate School of Natural and Applied Science, Ege University, Izmir, Türkiye
[3]Center for Drug R&D and Pharmacokinetic Applications (ARGEFAR), Ege University, Izmir, Türkiye
* yeliz.yildirim@ege.edu.tr
* Orcid No: 0000-0002-3014-4510

Received: 6 March 2024
Accepted: 27 June 2024
DOI: 10.18466/cbayarfbe.1448091

Abstract

Cafestol (CFS) is present in unfiltered coffee types and exhibits antidiabetic, anti-inflammatory and anticarcinogenic properties. The ionic gelation method was used to synthesise CFS-loaded chitosan (CS), and alginate (ALG) nanoparticles with high loading efficiency. The characterization, thermal properties and surface morphology of CFS-loaded biopolymer nanoparticles were carried out by FTIR, TGA and SEM, respectively. The encapsulation efficiency of the synthesised CFS-loaded biopolymer nanoparticles was found to be as 53% (CFS-loaded ALGNPs) and 92% (CFS-loaded CSNPs) by high-pressure liquid chromatography. The particle sizes determined using Malvern Zeta Sizer Ultra were 97 ± 4.04 (CFS-loaded CSNPs) and 81 ± 6.51 (CFS-loaded ALGNPs).

Keywords: Alginate, Cafestol, Chitosan, Drug Delivery Systems, Nanoparticle

1. Introduction

Coffee, a beverage widely consumed worldwide, is a complex substance that consists of various compounds. The structure of coffee indicates the presence of bioactive diterpene cafestol (CFS)/kahweol (CWL), which is one of the terpene species, as well as nearly 30 acids, such as chlorogenic and citric acids [1]. The biological properties of these compounds have been studied as a mixture of both because of the difficulty of isolating and separating CFS and CWL diterpenes from coffee as well as the unstable nature of CWL when purified [2]. Studies have focused on the antidiabetic, anti-inflammatory, and anticarcinogenic properties of CFS (Fig. 1).

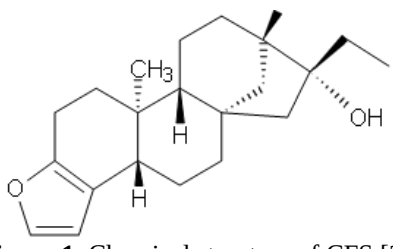

Figure 1. Chemical structure of CFS [2].

The anti-angiogenic effects of CFS palmitate and CWL palmitate (KP) were evaluated in an in-vitro animal model of angiogenesis. The results appeared that inhibited both compounds angiogenesis steps on human microvascular endothelial cells (HMVECs) [3]. In another study, INS-E1 rat insulin cells were used to investigate whether CFS increased insulin secretion from β cells in the short and long term. Insulin secretion increased by 12%–16% depending on the concentration in a 1-h exposure to CFS, and secretion increased by 34%–68% in a 72-h exposure. The results revealed that CFS may prevent Type-2 diabetes (T2D) in coffee drinkers [4]. Mellbye et al. investigated glucose uptake in cells and its effect on T2D by feeding male rats with a daily meal supplemented with 1.1 (high), 0.4 (low) or 0 (control) mg CFS for 10 weeks. At the end of the 10-week period, fasting plasma glucose was 28%–30% lower in the CFS groups than that in the control group, and insulin secretion increased by 75%–87% compared with the control group. CFS exhibits antidiabetic properties and can be used as a potential antidiabetic drug [5]. Studies have revealed that CFS exhibits antidiabetic properties [6] as well as anticarcinogen effects [7].

The head and neck cancer cells were treated with CFS and cisplatin to investigate whether CFS would increase the effectiveness of the chemotherapeutic agent cisplatin. Three cell lines, namely SCC25, CAL27 and FaDu, were used in the experiments, and depending on the dose, CFS inhibited carcinoma cell viability in all cell lines. Furthermore, in combination experiments using radiation, cells were first treated with CFS and subsequently irradiated. Although the combined treatment was effective in SCC25 and CAL27 cell lines, successful results were not obtained in the FaDu cell line [8]. A study evaluated the antitumor properties of CFS by examining its effect on four leukaemia cell lines, namely NB4, K562, HL60, and KG1 and revealed that it showed the highest cytotoxicity against HL60 and KG1 cells. The results showed that they were close to those obtained after the exposure of the HL60 cell line to the antileukemic drug cytarabine (Ara-C). Additionally, the co-treatment of CFS and Ara-C reduced HL60 cell viability compared to when either drug was given alone [9].

Lee et al. investigated the effects of CWL and CFS on oxidative stress and DNA damage in NIH3T3 cells. When NIH3T3 cells were treated with CWL and CFS, cytotoxicity, lipid peroxidation and production of reactive oxygen species reduced considerably in a dose-dependent manner. The results indicated that CWL and CFS could effectively protect against oxidative stress and DNA damage, and diterpenes functioned as antioxidants [10]. To combine the antibacterial and anti-inflammatory properties of zinc oxide nanoparticles with the antimicrobial properties of CFS, a chitosan (CS)-coated nanosystem was developed. The antibacterial activity of this system was investigated in Staphylococcus aureus, Bacillus cereus, Pseudomonas aeruginosa, and Escherichia coli bacteria, and the results revealed that ZnO, CS–ZnO and CFS-CS-ZnO nanoparticles inhibited the growth of S. aureus, B. cereus, and E. coli. The antibacterial activity was improved by coating CFS and ZnO nanoparticles with CS [11].

CS, obtained by the deacetylation of chitin is a biopolymer that exhibits excellent antibacterial, biorenewable, biocompatible, biodegradable, antimicrobial and antitumor properties [12,13]. Various types and combinations of CS as a drug delivery system have been investigated in studies such as doxorubicin-loaded CS nanobubbles [14], 5-fluorouracil-loaded CS microspheres [15], N-acetylcysteine-loaded CS-coated liposome [16], amiodoran-loaded CS nanoparticles [17], and Docataxel-loaded CS nanoparticles [18]. Nanoparticles have been preferred more than other carriers because of their high stability and high carrier capacity, facilitating the use of both hydrophilic and hydrophobic substances, and allowing controlled drug release [19].

Alginate (ALG) is a linear copolymer containing blocks of β–D-mannuronic acid and α-L-guluronic acid residues linearly linked by 1,4-glycosidic bonds and is a biocompatible polymer that is widely used in carrier systems as well as CS [20]. The presence of monomer units in ALG considerably influences drug release properties. The β–D-mannuronic acid groups provide excellent thickening, whereas the α-L-guluronic acid content contributes to superior gelling properties [20]. ALG nanoparticles also widely investigated for drug delivery systems as well, especially as anticarcinogenic drug carrier. One of the latest studies are, Docetaxel (DTX)-loaded sodium ALG nanoparticles used for to target colon cancer cells [21], Exemestane (EXE) drug used in breast cancer treatment was loaded on ALG nanoparticles [22], Cabazitaxel (CAB)-loaded poly(alkyl cyanoacrylate) (PACA) nanoparticles were encapsulated in alginate microspheres prepared aiming to delay anticancer drug absorption and reduce toxic side effects [23], and Sunitinib (STB) loaded alginate nanoparticles studied for enhancing oral bioavailability of STB which used for gastrointestinal stromal tumor [24]. Chlorhexidine loaded ALG nanoparticles also studied in dentistry for throat infection [25].

Within the scope of the study, it was aimed to load CFS (Fig. 1), which has been proven to exhibit anticancer, anti-inflammatory and antidiabetic properties, onto biocompatible polymer nanoparticles CS (CSNPs) and ALG (ALGNPs) and to carry out optimization and characterization studies of these biopolymer nanoparticles.

2. Materials and Methods

2.1. Materials

Low-molecular-weight CS powder (molecular weight: 50–190 kDa, 75%–85% deacetylated) and sodium ALG powder were obtained from Sigma-Aldrich Chemical Co. Ltd. Sodium tripolyphosphate (TPP) was procured from Alfa Aesar by Thermo Fisher Scientific, and CFS a crystalline solid, purity ≥98.0% obtained from Cayman Chemicals. All chemicals were analytical grade.

2.2. Equipments

A FTIR spectrometer (Spectrum Two, Pelkin Elmer, UK.) was used in the range 4000–500 cm^{-1}, and 10 scans were performed at a resolution of 4 cm^{-1} to detect the functional groups of all formulations. The nanoparticle samples were prepared with KBr pellets to analyse the chemical interactions between CFS and polymer matrix.

Average particle sizes were measured with multiangle dynamic light scattering using a Zetasizer (Malvern Instruments, Herrenberg, Germany). Purified water used as a medium for nanoparticle solution during analysis.

For the zeta potential same conditions were conducted and all analysis measured three times at 25°C.

The shape and surface morphology of CFS-loaded CSNPs, and CFS-loaded ALGNPs, were determined through scanning electron microscopy (SEM, Thermo Scientific Apreo S).

Thermogravimetric (TG) curves were obtained using a Diamond TG/DTA analyser (Pelkin Elmer, UK) from 30°C to 600°C, under a N_2 atmosphere at a 10°C/min heating rate for CFS-loaded nanoparticles.

2.3. Preparation of Nanoparticles

2.3.1 Preparation of CS Nanoparticles and CFS-loaded CS Nanoparticles (CSNPs / CFS-loaded CSNPs)

CSNPs were synthesized as described by Calvo et al. [26, 27]. CS (50 mg) was dissolved in the CH_3COOH (1% v/v ,25 ml) at room temperature under magnetic stirring until the formation of an opalescent suspension. The pH of the resulting solution was adjusted to 4.6–4.8 using the NaOH solution. CS nanoparticles were spontaneously obtained on the dropwise addition of TPP aqueous solution (CS to TPP weight ratio of 2:1 and TPP concentration is 7.5 mg/ml) to CS solution under constant magnetic stirring at room temperature. Nanoparticles were collected through centrifugation at 4°C before dried in a vacuum oven.

For preparing CFS-loaded CS nanoparticles, the CFS solution (100 µg/ml, 2 ml) was added before the TPP solution. The remaining processes were identical to the preparation of CS nanoparticles.

2.3.2 Preparation of ALG and CFS-loaded ALG Nanoparticles (ALGNPs/CFS-loaded ALG–NPs)

The method used to prepare ALG nanoparticles was modified from Rajaonarivony et al. [28]. Here, 2 mL of aqueous calcium chloride was added dropwise to 10 mL aqueous sodium ALG (3 mg/ml) with stirring at 1100 rpm. The nanoparticle solution stirred for 24h to obtain homogenous and uniform particle distribution. Nanoparticles were collected through centrifugation at 4°C before drying in a vacuum oven.

To prepare CFS-loaded alginate nanoparticles, the CFS solution (100 µg/ml, 2 ml) was added before the calcium chloride solution. The remaining processes were identical to the preparation of ALG nanoparticles.

2.4 HPLC

2.4.1 HPLC Conditions

The HPLC analysis method was modified from a previous study [29, 30]. The PDA detector HPLC system and the ACE C18 column (ACE; 250 × 4.6 mm, 5 µm) were used for the calibration curve of CFS. As the mobile phase, a mixture of acetonitrile and water was prepared at a ratio of 55:45 (v/v). The system was run with an isocratic flow rate of 0.9 mL/min rate, the injection amount was 20 µL, and the detector was set at 230 nm. The temperature of the column was 25°C, while the temperature for the autosampler was 30°C. In accordance with ICH guidelines Q2(R1), the present method was validated and found to be suitable for its intended purpose[31].

2.4.2 Preparation of stock solutions and standard working solutions

The stock solution of CFS (100 µg/mL) was prepared by dissolving 5.0 mg of drug in 50.0 mL ethanol. The standard solutions were stored at 4°C ± 1°C in a clear glass volumetric flask and lightly protected with an aluminium foil. The calibration curves of CFS concentrations of 0.5, 1.0, 5.0, 10.0, 20.0, 40.0, 60.0, 80.0 and 100.0 µL/mL in the working solution were determined. In the dilute solution, the stock solution was further diluted to make these working solutions daily. All samples were filtered through a 0.2 µm pore size filter (PTFE) followed by injection.

2.4.3 Calibration curve/Linearity

Analytical methods are linear when their results are directly proportional to variations in analyte concentration within a given range of concentrations or through a well-defined mathematical transformation. Linearity was analysed by plotting a calibration curve between concentration and areas obtained from standard solutions at ten different CFS concentrations (0.5–100.0 µg/mL in ethanol. Moreover, linearity was evaluated using least-square regression analysis, which utilizes a linear regression model.

2.4.4 Encapsulation efficiency

The encapsulation efficiencies (EE) of CFS-loaded CS, and ALG nanoparticles were determined after analysis in the HPLC (in triplicate) and calculated using the following equation:

$$\text{EE (\%)} = \frac{\textbf{Total amount of drug} - \textbf{Amount of free drug}}{\textbf{Total amount o f drug}} \text{ x } 100\ \%$$

3. Results and Discussion

CFS is a diterpene found in the structure of coffee, whose biological activities have been shown in various studies [4,5,6]. It was successfully encapsulated into CS and ALG biopolymers nanoparticles for the first time to ensure the continuity of the effectiveness of CFS for a long time. CFS-loaded CSNPs and CFS-loaded ALGNPs were synthesised by using the ionic gelation method with 64%, and 60% reaction yields, respectively.

Particle size and zeta potential of the synthesized nanoparticles were determined in solution using the DLS method. The results are revealed in Table 1. The results

obtained showed that the sizes of CSNPs and ALGNPs were 62 ± 3.92 and 61 ± 6.03 nm, by loading CFS into their structures, they increased to 97 ± 4.04 nm (for CFS-loaded CSNPs) and 81 ± 6.51 nm (for CFS-loaded ALGNPs). In the synthesis of CSNPs and ALGNPs, were founded that the synthesis conditions affect the size and reaction efficiency of the nanoparticle [32]. Therefore, optimisation studies investigated parameters, such as polymer molecular weight (low and medium molecular weight) and concentration, polymer-crosslinker ratio, pH, and drop rate were investigated. The results revealed that the size of the nanoparticle increased with the increase in the molecular weight and concentration of CS. Similarly, the particle size increased in the pH:5.5–5.6 range compared with pH 4.6–4.8. Kush et al. examined CS and TPP concentrations, CS:TPP ratios, temperature, mixing speed, and pH parameters to optimise the size of CSNPs. The CSNPs size were optimised as 159.2 ± 3.31 nm [33]. Çakır et al. (2020) investigated the effect of CS, TPP, Timol, Tween 80 concentrations and temperature parameters on the nanoparticle size in the synthesis of nanoparticles loaded with Timol and Tween 80 and revealed that the particle size increased with the increase in CS and TPP concentrations [34]. The optimum conditions for the synthesis of CFS-loaded CSNPs were low-molecular-weight CS concentration at 0.2 mg/ml; TPP concentration at 0.75 mg/ml; the pH was determined as a working range of 4.6–4.8 and a drop rate of 20 s. The particle size was 62 ± 3.92 nm for CSNPs and 97 ± 4.04 nm for CFS-loaded CSNPs (Table 1).

Sagis et al. (2014) investigated the effect of $CaCO_3$ and $CaCl_2$ crosslinkers on the size of ALG nanoparticles. The results of the study revealed that $CaCO_3$ was more effective than $CaCl_2$ as a crosslinker in reducing the particle size to nanoscale [35]. Mokhtari et al. (2017) studied the effect of the $CaCl_2$ concentration on the particle size and encapsulation efficiency in mint-phenolic-extract-loaded ALG nanospheres. The results revealed that the mean particle size decreased, and the encapsulation efficiency increased with the increase in the $CaCl_2$ concentration [36]. The optimum conditions were determined as 3.0 mg/mL ALG concentration, 3.35 mg/mL $CaCl_2$ concentration and the use of dripping rate every 20 s in our synthesis of CFS-loaded ALGNPs. Although the particle size was 61 ± 6.03 nm for ALGNPs, this value increased to 81 ± 6.51 nm for CFS-loaded ALGNPs (Table 1).

The zeta potentials of CFS-loaded biopolymer nanoparticles are shown in Table 1. Zeta potential, a physicochemical parameter expressing the stability of nanoformulations, is used to indirectly report the surface net charge. While extreme negative or positive values of zeta potential cause large repulsive forces, repulsion between particles with similar electrical charge prevents agglomeration. Depending on the suspension type, the distribution is a stable distribution system because of sufficient electrostatic repulsion between nanoparticles with a zeta potential of ±30 mV [37]. The zeta potentials for CSNPs, ALGNPs, CFS-loaded CSNPs and CFS-loaded ALGNPs were −25.8 ± 5.97 nm, −9.6 ± 4.67 nm, −10.2 ± 3.14 mV and −25.9 ± 1.82 mV, respectively (Table 1). According to the zeta potential results, the stability order of the synthesised CFS-loaded polymer NPs in our study was ALGNPs < CFS-loaded CSNPs < CSNPs < CFS-loaded ALGNPs.

Table 1. Particle sizes, Zeta potentials, and encapsulation efficiencies of CSNPs, ALGNPs, ALG–CSNPs, and CFS-loaded nanoparticles.

Formulation Code	Particle Size (nm)	Zeta Potential (mV)	Encapsulation Efficiency (%)
CSNPs	62 ± 3.92	−25.8 ± 5.97	-
CFS-loaded CSNPs	97 ± 4.04	−10.2 ± 3.14	92 ± 2.1
ALGNPs	61 ± 6.03	−9.6 ± 4.67	-
CFS-loaded ALGNPs	81 ± 6.51	−25.9 ± 1.82	53 ± 1.8

Bakhshi et al. (2017) reported the zeta potentials of ALGNPs and immunoglobulin-loaded ALGNPs as −26.8 and −36.9 mV, respectively. They concluded that the negative surface charge of sodium ALGNPs can be attributed to the presence of carboxyl groups of ionised alginate molecules on the surface of nanoparticles. The zeta potential parameter represents the high surface charge of nanoparticles, which results in strong repulsive interactions between nanoparticles in dispersion [38]. Spadari et al. revealed that the zeta potential values of ALGNPs and miltefosine-loaded ALGNPs were measured to be −36.2 ± 6.8 and −39.7 ± 5.2 mV, respectively. They also reported that the uptake of negatively charged nanoparticles into the cell by the mucosa occurs through the nonspecific adsorption process of nanoparticles on the cell membrane and the formation of nanoparticle aggregates [39].

Consequently, according to the zeta potential results, the stability order of the synthesised CFS-loaded polymer NPs in our study was CFS-loaded CSNPs (−10.2 ± 3.14) < CFS-loaded ALGNPs (−25.9 ± 1.82).

3.1 Encapsulation Efficiency

The amount of free CFS from the reaction medium after synthesis was determined using the HPLC analysis method under PDA detector, the ACE C18 column (ACE; 250 × 4.6 mm, 5 µm) the mobile phase which contains a mixture of acetonitrile and water at a ratio of 55:45 (v/v) conditions in order to determine the encapsulation efficiency. Figure 2 shows the calibration chart drawn in ethanol environment.

Celal Bayar University Journal of Science
Volume 20, Issue 4, 2024, p 72-81
Doi: 10.18466/cbayarfbe.1448091

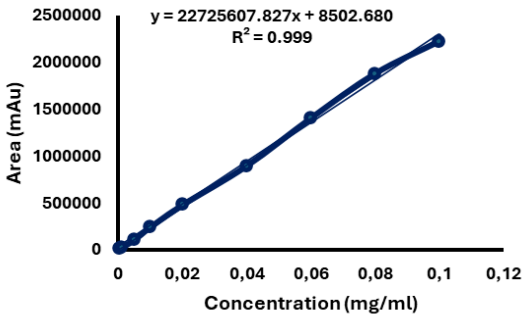

Figure 2. Calibration curve of CFS in ethanol.

The encapsulation efficiencies of CFS to CSNP and ALGNP were calculated by using free CFS amounts obtained the HPLC analyses results. The encapsulation efficiency of CFS-loaded CSNPs and CFS-loaded ALGNPs are found 92 ± 2.1 and 53 ± 1.8, respectively. The obtained results are summarized in Table 1.

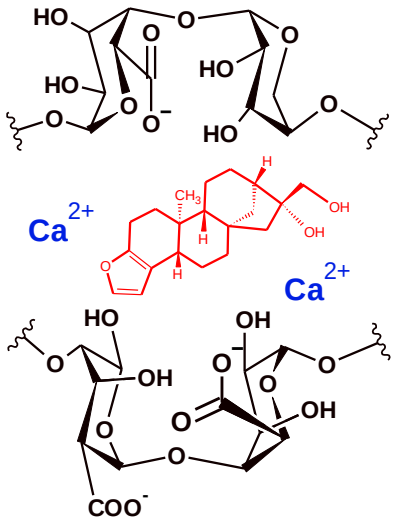

Figure 3. Probable interaction between ALG and $CaCl_2$.

The encapsulation efficiency of CS nanoparticles is 1.75 times higher than that of ALG nanoparticles. When the molecular structures are examined, it is possible that the protonated amine groups in the structure of CS interact with the partial negative OH groups in the structure of CFS. On the other hand, the negative OH groups in the structure of the ALG polymer are expected to have a reducing effect on the encapsulation of CFS into the polymeric nanoparticle There are some studies in the literature that predict the interaction between CS with TPP and ALG with $CaCl_2$ [40, 41]. In the light of these studies, the possible interactions between CFS to ALGNP or CSNP are shown in Figures 3 and 4, respectively.

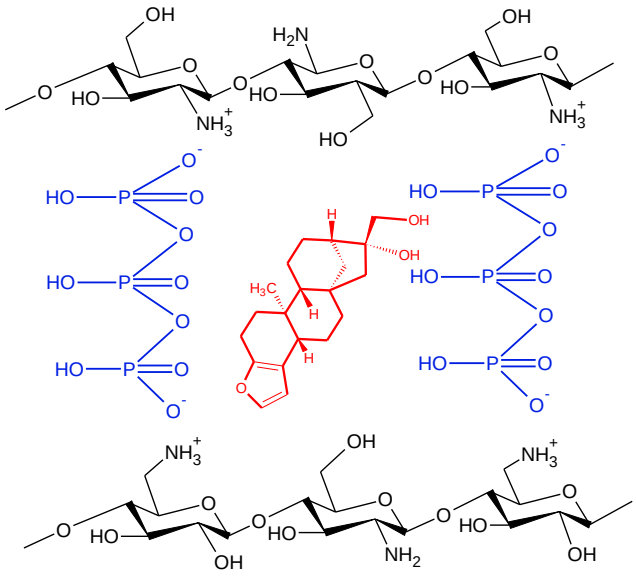

Figure 4. Probable interaction between Chitosan (CS) NPs and CFS.

3.1 FTIR analysis

The spectra of pure CFS, pure CS, pure ALG, CSNPs, ALGNPs, CFS-loaded CSNPs and CFS-loaded ALGNPs obtained by using FTIR spectroscopy to confirm CFS-loaded nanoparticles (Figures 5, and 6).

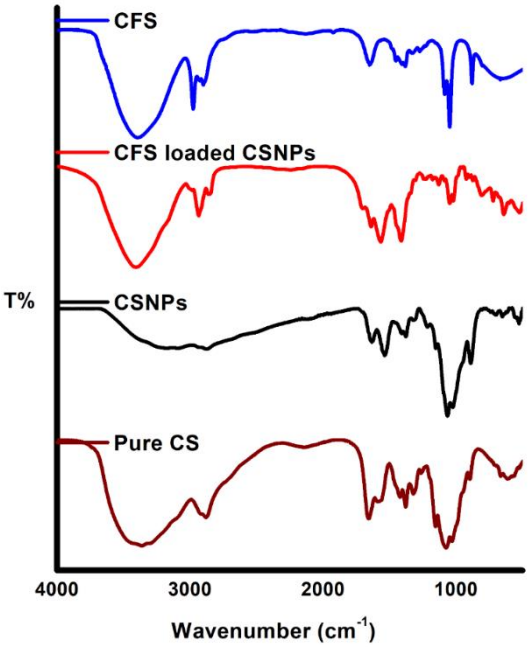

Figure 5. FTIR spectra of pure CS, pure CFS, CSNPs and CFS loaded CSNPs.

The FTIR spectra of pure CS, pure CFS, CSNPs and CFS loaded CSNPs are displayed in Figure 5. The peak at 3500–3200 cm^{-1} was attributed to $–NH_2$ and –OH groups. This broad peak was attributed to the increased

hydrogen bonding in CSNPs resulting from the interaction between the NH_3 group of CS and the $P_2O_5^{-1}$ group of TPP (Figure 4). The peaks at 1624 and 1532 cm^{-1} can be interpreted as the N–H vibration of the $–NH_3^+$ group and the C-H vibration of the alkyl group, respectively. The absorption peaks approximately 1083 and 890 cm^{-1} may be attributed to C–O–C anti-symmetric stretching at the β-(1-4)-glycosidic linkages of CS [42].

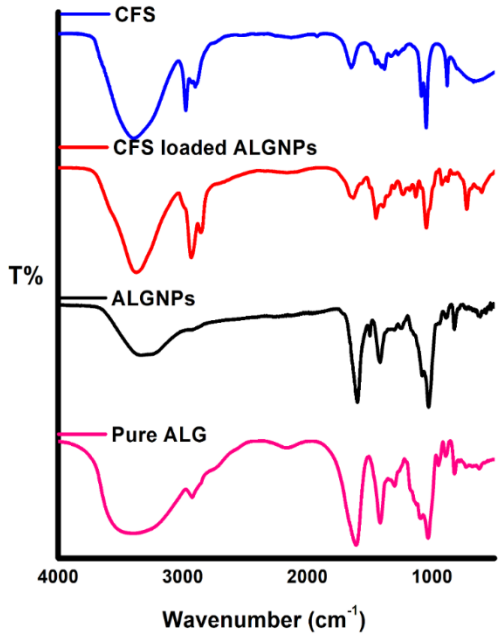

Figure 6. FTIR spectra of pure ALG, pure CFS, ALGNPs and CFS loaded ALGNPs.

The pure CFS spectrum displays the presence of the broad band –OH group and H bonds in the range 3100–3500 cm^{-1}. In the spectra pure CFS, typical peaks were detected at 2974, 1650, 1381 cm^{-1} for =C−H stretching, the C=C group, and the Aryl CH_3 group. The peaks at 1085, 1049 and 880 cm^{-1} was attributed to C–O–C and C–O stresses in the furan ring [11, 43]. The OH band between 3000–3700 cm^{-1} was intensified in the CFS-loaded CSNPs spectrum. The peak at 2974 cm^{-1} in the molecular spectrum in CFS shifted to 2937 cm^{-1} in the CFS-loaded CSNPs spectrum. The peaks of C–O–C and C–O stretching vibration at 1085 and 1049 cm^{-1} in CFS spectra shifted to 1047 and 1021 cm^{-1} in the CFS-loaded CSNPs spectrum. Compared with the pure CFS, absorption peaks at the fingerprint region (1600–400 cm^{-1}) were observed in CFS-loaded CSNPs, which indicated successful entrapment of CFS inside CSNPs.
Figure 6 depicts the FTIR spectra of the pure ALG, pure CFS, ALGNPs and CFS loaded ALGNPs. The characteristic peak of the –OH functional group in the structure of the ALG polymer and the stretching vibration band of the hydrogen bond between the -OH and -COOH groups exhibits a wide peak in the range 3000–3600 cm^{-1}. The bands at 1599, 1493 and 1416 cm^{-1} also revealed asymmetric and symmetric stretching vibrations of the carboxyl group. The bands at 1080 and 1029 cm^{-1} were the tension vibration bands of the C–O band in the C–OH of the sugar group. The FTIR spectrum of ALGNPs revealed characteristic bands between 3000 and 3600 (OH stretching vibrations), 2924 (CH stretching vibrations), and 1080 cm^{-1} (COC stretching vibrations). FTIR spectra obtained for ALG and ALGNPs were compatible with those of literature values [44;45]. The OH band intensified in the spectrum of CFS-loaded ALGNPs, and the peaks at 2974 and 2901 cm^{-1} in CFS shifted to 2933 and 2860 cm^{-1}. The peak of C–O–C stresses shifted from 882 to 723 cm^{-1} wavelength. The peak CFS at 1047 cm^{-1}, which corresponds to the presence of the C–O peak in the furan ring, was loaded on ALGNPs.

3.2 TG analysis

The Perkin–Elmer Diamond TG/DTA analyser was used to investigate the thermal behaviours of the synthesised CFS-loaded CSNPs, and ALGNPs. TG analyses were obtained from 30°C to 600°C with a heating rate of 10°C min^{-1} under N_2 atmosphere with a flow rate of 20 ml/min. The TG and DTG of pure CS, CSNPs, and CFS-loaded CSNPs are displayed in Figures 7 and 8, respectively. The T_{onset}, T_{max}, and residual at 600°C are displayed in Table 2.

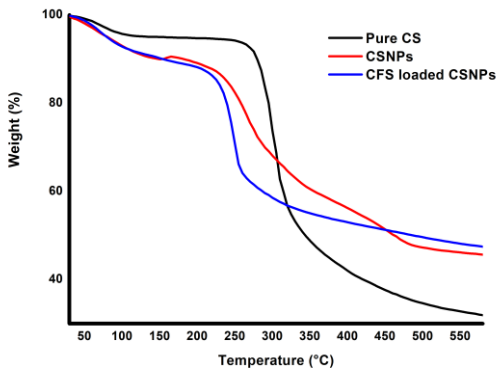

Figure 7. Thermogravimetric (TG) curves of pure CS, CSNPs, CFS-loaded CSNPs.

The TG curve of pure CS (Figure 7) revealed that the two stages of weight loss ranged from 60°C to 480°C. The first occurring weight loss in the range 60°C–120°C could be attributed to water desorption with a weight loss of approximately 6%. The primary degradation of pure CS started at 245°C and completely degraded at approximately 480°C with a weight loss of approximately 58%. Corazzari et al. examined the thermal behaviour of pure CS and obtained the thermogram similar to our study [46]. The main mass loss occurring between 245°C and 480°C could be attributed to the separation of H_2O, NH_3, CO, CO_2 and CH_3COOH groups because of CS pyrolysis [47]. Comparisons of the

thermograms of pure CS and CSNPs revealed that their thermal behaviour changed (Figure 7 and Table 2).

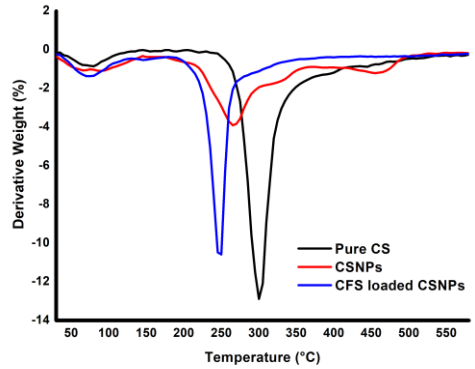

Figure 8. Derivative thermogravimetry (DTG) curves of Pure CS, CSNPs, and CFS-loaded CSNPs.

Table 2 Thermal parameters derived from TG (T_{onset}, T_{max}, and residual mass (%) at 600 °C) for pure CS, CSNPs, and CFS-loaded CSNPs**.**

Sample	T_{onset} (°C)	T_{max} (°C)	Residual (%) at 600°C
Pure CS	245	300	32
CSNPs	165	235	47
CFS-loaded CSNPs	165	245	48

Figure 7 revealed that approximately 10% water loss in CSNPs occurred in the range 60°C–120°C. The 40% mass loss in CSNPs between 165°C and 480 °C could be attributed to the dehydration of the saccharide rings, depolymerisation, and decomposition of acetylated and deacetylated units [48]. The thermograms of CFS-loaded CSNPs revealed a shift in the second degradation step of nanoparticles compared with CSNPs. This shift could be attributed to the interaction between CFS and the polymeric matrix as well as disturbances in the crystal structure of the nanoparticles. Michaillidou et al. revealed a similar observation in the thermograms of Budesonide-loaded CSNPs [49]. The difference in the thermograms of CFS-loaded CSNPs and CSNPs indicated that CFS was loaded on CSNPs.

The TG and DTG of pure ALG, ALGNPs and CFS-loaded ALGNPs are displayed in Figures 9 and 10, respectively. Table 3 depicts the T_{onset}, T_{max}, and residual at 600°C.

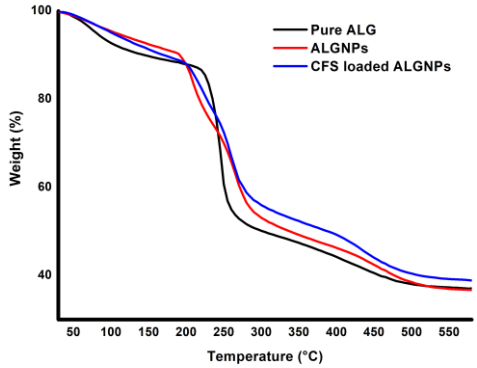

Figure 9. TG curves of pure ALG, ALGNPs and CFS-loaded ALGNPs.

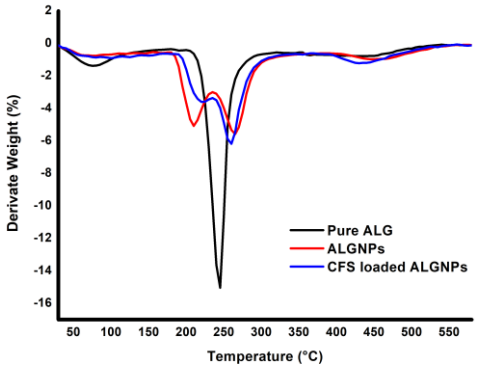

Figure 10. DTG curves of pure ALG, ALGNPs and CFS-loaded ALGNPs.

Table 3 Thermal parameters derived from TG (T_{onset}, T_{max}, and residual mass (%) at 600°C) for pure ALG, ALGNPs and CFS-loaded ALGNPs.

Sample	T_{onset} (°C)	T_{max} (°C)	Residual (%) at 600°C
Pure ALG	200	245	37
ALGNPs	170	210/265/465	37
CFS-loaded ALGNPs	185	225/260/440	39

Figure 9 displays the TG of pure ALG. The TG of pure ALG revealed a three-step weight loss. The initial weight loss of approximately 11% at 60°C–130°C was attributed to the evaporation of moisture and residual water present in the sample. The second degradation stage can be interpreted as crosslinking of polymer networks in the temperature range 200°C–280°C with 38% weight loss. The last decomposition step was interpreted as Na_2CO_3 char formation, which consisted of the structure of sodium ALG polymer [50]. Salisu et al. interpreted the second decomposition step occurring between 200°C–250°C in the thermogram for the ALG polymer to be the

formation of water, CH_4 and CO_2 gas [51]. Figure 10 displays four degradation stages occurring in ALG nanoparticles. The first decomposition stage between 60°C–130°C had 8% moisture loss, the second decomposition at 180°C–240°C had a mass loss of 16%, and the third decomposition at 240°C–280°C had a mass loss of 19%. The final decomposition occurred between the temperatures of 380°C–510°C with a mass loss of 9%. The thermogram results are similar to calcium ALGNPs thermograms obtained by Gokila et al. [52]. Figure 9 displays the TG thermogram of CFS-loaded ALGNPs. Four degradation steps occurred in the thermogram. The initial weight loss of approximately 8% exhibited at 60°C–130°C was attributed to the residual water in the sample. Comparison of the thermograms of ALGNPs and ALGNPs with CFS-loaded ALGNPs revealed that the second, third, and fourth steps slightly shifted to 190°C–235°C with 12% mass loss, to 235°C–280°C with 8% mass loss, and to 390°C–530°C with 9% mass loss, respectively. The shifts in the T_{max} values of CFS-loaded ALGNPs and ALGNPs in Table 3 are interpreted as the result of electrostatic interactions between ALGNPs and CFS. Güncüm et al. synthesised amoxicillin loaded PVA/NaAlg nanoparticles. The thermograms of these nanoparticles shifted with drug loading on ALGNPs as observed in our study [53]. Thus, differences in the thermal characterisation of CFS-loaded ALGNPs and ALGNPs thermograms indicated that CFS was loaded on ALGNPs.

3.3 SEM analysis

The SEM images of CSNPs, ALGNPs, CFS-loaded CSNPs, and ALGNPs are displayed in Figure 11 a-d. SEM analysis provides information of the morphology of the synthesised structures, and the sizes obtained were closer to reality than DLS measurements. DLS determines the apparent size (hydrodynamic radius) of a particle, including hydrodynamic layers formed around hydrophilic particles DLS analysis conducted in a solvent, which is mostly water, medium and as a result given particle size includes solvent molecules size as well. Which lead to an overestimation of the nanoparticle size [54].

When studies have investigated CFS-loaded and CSNPs, and ALGNPs as drug delivery systems, SEM images were obtained to examine the surface morphology. ALGNPs synthesised by various methods such as emulsification/internal gelation, spray dryer, polyelectrolyte complexation, emulsification/external gelation, and evaporation method had a spherical structure [32]. Sarei et al. (2013) reported that ALGNPs were synthesised as a vaccine carrier system for diphtheria with a high loading capacity of 70 ± 0.5 nm in size and spherical morphology [55]. Nallamuthu et al. (2015) revealed that chlorogenic-acid-loaded CSNPs synthesised by the ionic gelation method were homogeneous and spherical [56]. The SEM images of CFS-loaded CSNPs, and ALGNPs revealed that they had similar spherical morphology and were smaller than 100 nm. Therefore, the morphologies of CFS-loaded CSNPs, and ALGNPs, were consistent with the studies in the literature investigating drug carrier systems, such as CSNPs, and ALGNPs.

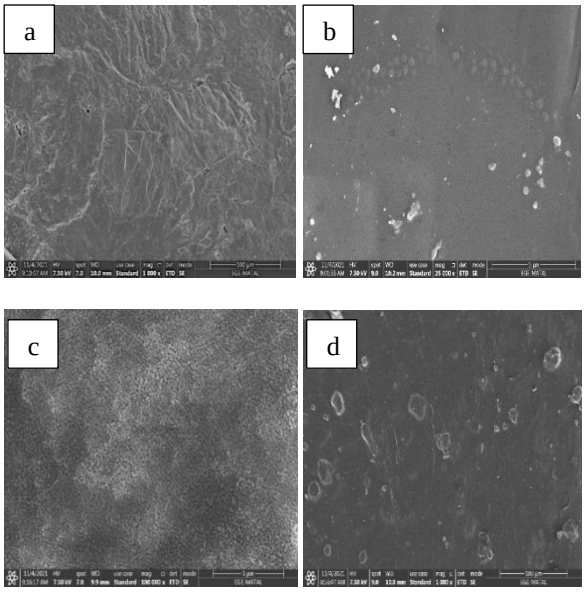

Figure 11. Scanning electron microscopy (SEM) images of a: CSNPs (x 1000), b: CFS-loaded CSNPs (x 25000), c: ALGNPs (x1000), d: CFS-loaded ALGNPs (x 1000).

4. Conclusion

CFS active ingredient found in coffee beans with antidiabetic, anticarcinogenic, and anti-inflammatory properties was loaded into biopolymers nanoparticles such as CS and ALG. CFS-loaded biopolymer nanoparticles were synthesized using the ionic gelation method in high reaction yield. FTIR, TG, SEM and HPLC analysis were performed to characterise CFS-loaded biopolymer nanoparticles. SEM analysis revealed that CFS-loaded CSNPs, and ALGNPs were spherical. Furthermore, FTIR and TG analysis disclosed that CFS was loaded into biopolymer nanoparticles. As a result of HPLC analysis, it is seen that the loading efficiency of CFS on CS nanoparticles is 1.75 times higher than that of ALG nanoparticles. When examined in terms of stability, it was concluded that ALGNPs were more stable in terms of zeta potential. As a continuation of the study, it is planned to conduct in vitro release and cell culture experiments of CFS-loaded polymeric nanoparticles to compare their antidiabetic and anticarcinogenic properties with free CFS.

Acknowledgement

This research is supported by grants from the Ege University Scientific Research Coordination Office (Project No. 21692).

Author's Contributions

Özge VARDAR and Ayça MEHMETOĞLU AL: investigation, conducted experiments, validation, writing-original draft.

Yeliz YILDIRIM: writing, review and editing-original draft, supervision, project administration, funding acquisition.

Ethics

There are no ethical issues after the publication of this manuscript.

References

[1]. George S.E; Ramalakshmi K.; Mohan Rao LJ. (2008) A perception on health benefits of coffee. Crit Rev Food Sci Nutr 48, 464-486.

[2]. Ren Y.; Wang C.; Xu J.; Wang S. (2019) Cafestol and kahweol: A review on their bioactivities and pharmacological properties. Int J Mol Sci 20, 4238.

[3]. Moeenfard M.; Cortez A.; Machado V.; et al. (2016) Anti-angiogenic properties of Cafestol and Kahweol palmitate diterpene esters. J Cell Biochem 117, 2748-2756.

[4]. Mellbye F.B.; Jeppesen P.B.; Hermansen K.; Gregersen S. (2015) Cafestol, a bioactive substance in coffee, stimulates insulin secretion and increases glucose uptake in muscle cells: studies in vitro. J Nat Prod 78, 2447-2451.

[5]. Mellbye F.B.; Jeppesen P.B.; Shokouh P.; et al. (2017) Cafestol, a bioactive substance in coffee, has antidiabetic properties in KKAy mice. J Nat Prod 80, 2353-2359.

[6]. Loureiro L.M.R.; Reis C.E.G.; da Costa T.H.M. (2018) Effects of coffee components on muscle glycogen recovery: a systematic review. Int J Sport Nutr Exerc Metab 28, 284-293.

[7]. Moolgavkar S.H. (1978) The multistage theory of carcinogenesis and the age distribution of cancer in man. J Natl Cancer Inst 61, 49-52.

[8]. Kotowski U.; Heiduschka G.; Seemann R.; et al. (2015) Effect of the coffee ingredient cafestol on head and neck squamous cell carcinoma cell lines. Strahlenther Onkol 191, 511-517.

[9]. Lima C.S.; Spindola D.G.; Bechara A.; et al. (2017) Cafestol, a diterpene molecule found in coffee, induces leukemia cell death. Biomed Pharmacother 92, 1045-1054.

[10]. Lee K.J.; Choi J.H.; Jeong H.G. (2007) Hepatoprotective and antioxidant effects of the coffee diterpenes kahweol and cafestol on carbon tetrachloride-induced liver damage in mice. Food Chem Toxicol 45, 2118-2125.

[11]. Ballıca G.; Çevikbaş H.; Ulusoy S.; Yıldırım Y. (2020) The synthesis of novel Cafestol loaded zinc oxide nanoparticles and their characterization. Appl Nanosci 10, 4263-4272.

[12]. Thomas S.; Pius A.; Gopi S. (2020) Handbook of Chitin and Chitosan: Volume 2: Composites and Nanocomposites from Chitin and Chitosan, Manufacturing and Characterisations. Elsevier.

[13]. Zargar V.; Asghari M.; Dashti A. (2015) A review on chitin and chitosan polymers: structure, chemistry, solubility, derivatives, and applications. Chem Bio Eng Reviews 2, 204-226.

[14]. Zhou X.; Guo L.; Shi D.; Duan S.; Li J. (2019) Biocompatible chitosan nanobubbles for ultrasound-mediated targeted delivery of doxorubicin. Nanoscale Res Lett 14, 1-9.

[15]. He T.; Wang W.; Chen B.; Wang J.; Liang Q.; Chen B. (2020) 5-Fluorouracil monodispersed chitosan microspheres: Microfluidic chip fabrication with crosslinking, characterization, drug release and anticancer activity. Carbohydr Polym 236, 116094.

[16]. Hamedinasab H.; Rezayan A.H.; Mellat M.; Mashreghi M.; Jaafari M.R. (2020) Development of chitosan-coated liposome for pulmonary delivery of N-acetylcysteine. Int J Biol Macromol 156:1455-1463.

[17]. Buyuk N.I.; Arayici P.P.; Derman S.; Mustafaeva Z.; Yucel S. (2020) Synthesis of chitosan nanoparticles for controlled release of amiodarone. Indian J Pharm Sci 82:131-138.

[18]. Gelperina S.; Kisich K.; Iseman M.D.; Heifets L. (2005) The potential advantages of nanoparticle drug delivery systems in chemotherapy of tuberculosis. Am J Respir Crit Care Med 172, 1487-1490.

[19]. Paques J.P.; van der Linden E.; van Rijn C.J.; Sagis L.M. (2014) Preparation methods of alginate nanoparticles. Adv Colloid Interface Sci 209:63-171.

[20]. Chiu H.I.; Ayub A.D.; Mat Yusuf S.N.A.; et al. (2020) Docetaxel-loaded disulfide cross-linked nanoparticles derived from thiolated sodium alginate for colon cancer drug delivery. Pharmaceutics 12(1), 1-25.

[21]. Jayapal J.J.; Dhanaraj S. (2017) Exemestane loaded alginate nanoparticles for cancer treatment: Formulation and in vitro evaluation. Int J Biol Macromol 105, 416-421.

[22]. Fleten, K. G., Hyldbakk, A., Einen, C., Benjakul, S., Strand, B. L., Davies, C. D. L., ... & Flatmark, K. (2022) Alginate Microsphere Encapsulation of Drug-Loaded Nanoparticles: A Novel Strategy for Intraperitoneal Drug Delivery. Marine Drugs 20(12), 744.

[23]. Joseph, J. J., Sangeetha, D., & Shivashankar, M. (2019) In vitro release and cytotoxic studies of novel alginate nanocarrier for the antitumor drug: Sunitinib. Regen Eng Transl Med, 5, 220-227.

[24]. Rai, V. K., Kumar, A., Pradhan, D., Halder, J., Rajwar, T. K., Sarangi, M. K., ... & Rath, G. Spray-Dried (2024) Mucoadhesive Re-dispersible Gargle of Chlorhexidine for Improved Response Against Throat Infection: Formulation Development, In Vitro and In Vivo Evaluation. AAPS PharmSciTech, 25(2), 31.

[25]. Calvo P.; Remuñan-López C.; Vila-Jato J.L.; Alonso M.J. (1997) Chitosan and chitosan/ethylene oxide-propylene oxide block copolymer nanoparticles as novel carriers for proteins and vaccines. Pharm Res 14, 1431-1436. 25.2

[26]. Vila A.; Sánchez A.; Janes K et al. (2004) Low molecular weight chitosan nanoparticles as new carriers for nasal vaccine delivery in mice. Eur J Pharm Biopharm 57, 123-131.

[27]. Rajaonarivony M.; Vauthier C.; Couarraze G.; Puisieux F.; Couvreur P. (1993) Development of a new drug carrier made from alginate. J Pharm Sci 82, 912-917.

[28]. Dias R.C.E.; Campanha F.G.; Vieira L.G.E et al. (2010) Evaluation of kahweol and cafestol in coffee tissues and roasted coffee by a new high-performance liquid chromatography methodology. J Agric Food Chem 58, 88-93.

[29]. Silva J.A.; Borges N.; Santos A.; Alves A. (2012) Method validation for cafestol and kahweol quantification in coffee brews by HPLC-DAD. Food Anal Methods 5, 1404–1410.

[30]. Guideline IHT (2005) Validation of analytical procedures: text and methodology. Q2 (R1), 1(20), 05.

[31]. Oh J.W.; Chun S.C.; Chandrasekaran M. (2019) Preparation and in vitro characterization of chitosan nanoparticles and their broad-spectrum antifungal action compared to antibacterial activities against phytopathogens of tomato. Agron J 9(1), 21.

[32]. Jain A.; Thakur K.; Sharma G.; Kush P.; Jain U.K. (2016) Fabrication, characterization and cytotoxicity studies of ionically cross-linked docetaxel loaded chitosan nanoparticles. Carbohydr Polym 137, 65-74.

[33]. Çakır M.A.; Icyer N.C.; Tornuk F. (2020) Optimization of production parameters for fabrication of thymol-loaded chitosan nanoparticles. Int J Biol Macromol 151, 230-238.

[34]. Paques J.P.; Sagis L.M.; van Rijn C.J.; van der Linden E. (2014) Nanospheres of alginate prepared through w/o emulsification and internal gelation with nanoparticles of CaCO3. Food Hydrocoll 40, 182-188.

[35]. Mokhtari S.; Jafari S.M.; Assadpour E. (2017) Development of a nutraceutical nano-delivery system through emulsification/internal gelation of alginate. Food Chem 229, 286-295.

[36]. Lunardi C.N.; Gomes A.J.; Rocha F.S.; De Tommaso J.; Patience G.S. (2021) Experimental methods in chemical engineering: Zeta potential. Can J Chem Eng 99, 627–639.

[37]. Bakhshi M.; Ebrahimi F.; Nazarian S et al. (2017) Nano-encapsulation of chicken immunoglobulin (IgY) in sodium alginate nanoparticles: In vitro characterization. Biologicals 49, 69-75.

[38]. de Castro Spadari C. (2019) Alginate nanoparticles as non-toxic delivery system for miltefosine in the treatment of candidiasis and cryptococcosis. Int J Nanomed 14, 5187.

[39]. Sarei F.; Dounighi N.M., Zolfagharian H.; Khaki P.; Bidhendi S.M. (2013) Alginate nanoparticles as a promising adjuvant and vaccine delivery system. Indian J Pharm Sci 75, 442.

[40]. Silvestro, I., Francolini, I., Di Lisio, V., Martinelli, A., Pietrelli, L., Scotto d'Abusco, A., ... & Piozzi, A. (2020). Preparation and characterization of TPP-chitosan crosslinked scaffolds for tissue engineering. Materials, 13(16), 3577.

[41]. Costa, M. J., Marques, A. M., Pastrana, L. M., Teixeira, J. A., Sillankorva, S. M., & Cerqueira, M. A. (2018). Physicochemical properties of alginate-based films: Effect of ionic crosslinking and mannuronic and guluronic acid ratio. Food hydrocolloids, 81, 442-448.

[42]. Terrile E.A.; Marcheafave G.G.; Oliveira S.G et al. (2016) Chemometric analysis of UV characteristic profile and infrared fingerprint variations of coffea Arabica green beans under different space management treatments. J Braz Chem Soc 27, 1254-1263.

[43]. Derkus B.; Emregul E., Emregul K.C.; Yucesan C. (2014) Alginate and alginate-titanium dioxide nanocomposite as electrode materials for anti-myelin basic protein immunosensing. Sens Actuators B Chem 192, 294-302.

[44]. El-Shamy O.A.; El-Azabawy R.E.; El-Azabawy O. (2019) Synthesis and characterization of magnetite-alginate nanoparticles for enhancement of nickel and cobalt ion adsorption from wastewater. J Nanomater Article ID 6326012:1-8

[45]. Brito D.; Campana-Filho S.P. (2007) Kinetics of the thermal degradation of chitosan. Thermochim Acta 465, 73-82.

[46]. Corazzari I.; Nisticò R.; Turci F et al. (2015) Advanced physico-chemical characterization of chitosan by means of TGA coupled on-line with FTIR and GCMS: Thermal degradation and water adsorption capacity. Polym Degrad Stab 112, 1-9.

[47]. Zhang H.; Zhao Y. (2015) Preparation, characterization and evaluation of tea polyphenol–Zn complex loaded β-chitosan nanoparticles. Food Hydrocoll 48, 260-273.

[48]. Michailidou G.; Ainali N.M.; Xanthopoulou E et al. (2020) Effect of poly (vinyl alcohol) on nanoencapsulation of budesonide in chitosan nanoparticles via ionic gelation and its improved bioavailability. Polym J 12, 1101-1023.

[49]. Swamy T.M.; Ramaraj B.; Lee J.H. (2008) Sodium alginate and its blends with starch: thermal and morphological properties. J Appl Polym Sci 109, 4075-4081.

[50]. Salisu A.; Sanagi M.M.; Abu Naim A et al. (2016) Alginate graft polyacrylonitrile beads for the removal of lead from aqueous solutions. Polym Bull 73, 519-537.

[51]. Gokila S.; Gomathi T.; Sudha P.N.; Anil S. (2017) Removal of the heavy metal ion chromiuim (VI) using Chitosan and Alginate nanocomposites. Int J Biol Macromol 104, 1459-1468.

[52]. Güncüm E.; Işıklan N.; Anlaş C et al. (2018) Development and characterization of polymeric-based nanoparticles for sustained release of amoxicillin–an antimicrobial drug. Artif Cells Nanomed Biotechnol 46, 964-973.

[53]. Bootz A.; Vogel V.; Schubert D.; Kreuter J. (2004) Comparison of scanning electron microscopy, dynamic light scattering and analytical ultracentrifugation for the sizing of poly (butyl cyanoacrylate) nanoparticles. Eur J Pharm Biopharm 57, 369-375.

[54]. Daemi H.; Barikani M. (2012) Synthesis and characterization of calcium alginate nanoparticles, sodium homopolymannuronate salt and its calcium nanoparticles. Sci Iran 19, 2023-2028.

[55]. Gazori T.; Khoshayand M.R.; Azizi E et al. (2009) Evaluation of alginate/chitosan nanoparticles as antisense delivery vector: formulation, optimization and in vitro characterization. Carbohydr Polym. 77, 599-606.

[56]. Nallamuthu I.; Devi A.; Khanum F. (2015) Chlorogenic acid loaded chitosan nanoparticles with sustained release property, retained antioxidant activity and enhanced bioavailability. Asian J Pharm Sci 10, 203-211.